frontiers in Earth Science

ORIGINAL RESEARCH
published: 04 June 2021
doi: 10.3389/feart.2021.656281

Holocene Lake Evolution and Glacial Fluctuations Indicated by Carbonate Minerals and Their Isotopic Compositions in the Sediments of a Glacial Melt Recharge Lake on the Northwestern Tibetan Plateau

Minghui Li[1,2], Liping Zhu[1,2,3], Junbo Wang[1,2], Jianting Ju[1], Chong Liu[1,3], Qingfeng Ma[1], Teng Xu[1,3], Baojin Qiao[4] and Xiaoxiao Wang[1,3]*

[1]Key Laboratory of Tibetan Environment Changes and Land Surface Processes, Institute of Tibetan Plateau Research, Chinese Academy of Sciences, Beijing, China, [2]CAS Center for Excellence in Tibetan Plateau Earth Sciences, Beijing, China, [3]University of Chinese Academy of Sciences, Beijing, China, [4]School of Geosciences and Technology, Zhengzhou University, Zhengzhou, China

Lakes and glaciers are widely distributed on the Tibetan Plateau and are linked via hydrological processes. They are experiencing rapid changes due to global warming, but their relationships during the Holocene are less well known due to limited coupled geological records. Here, we analyzed the $\delta^{13}C_{\text{-VPDB}}$ and $\delta^{18}O_{\text{-VPDB}}$ values and ion content of calcite and aragonite in a 407-cm-long sediment core from Guozha Co, a closed basin on the northwestern Tibetan Plateau supplied by glacial meltwater, in order to understand how the lake responded to glacier changes during the Holocene. Our results indicate that the glacial meltwater lowered the lake's temperature and the $\delta^{18}O_{\text{lake water}}$ and $\delta^{18}O_{\text{endogenic + authigenic carbonate}}$ values and diluted the ion concentrations in the lake water. Three stages of evolution, 8.7–4.0, 4.0–1.5, and 1.5 kyr BP to present, are distinguished based on the decrease in glacial meltwater recharge. Guozha Co has been a closed basin since at least 8.7 kyr BP, and it has changed from a fresh water lake during 8.7–1.5 kyr BP to a brackish lake from 1.5 kyr BP to present due to several climate events. The famous 4.2 kyr BP cold event was identified in the core at 4.0 kyr BP, while warm events occurred at 6.2, 3.9, 2.2, 0.9, and 0.4 kyr BP. Both glaciers and lakes in this area are controlled by climate, but they exhibit opposite changes, that is, glaciers retreat and lakes expand, and vice versa. Our results provide an accurate interpretation of the cold events based on carbonate minerals and carbon–oxygen isotopes in glacial meltwater–recharged lake sediments.

Keywords: carbonate minerals, oxygen and carbon isotopes, lake water temperature, glacial fluctuations, climatic events

OPEN ACCESS

Edited by:
Praveen K. Mishra, Wadia Institute of Himalayan Geology, India

Reviewed by:
Som Dutt, Wadia Institute of Himalayan Geology, India
Sayak Basu, Indian Institute of Science Education and Research Mohali, India

***Correspondence:**
Liping Zhu
lpzhu@itpcas.ac.cn

Specialty section:
This article was submitted to Quaternary Science, Geomorphology and Paleoenvironment, a section of the journal Frontiers in Earth Science

Received: *20 January 2021*
Accepted: *10 May 2021*
Published: *04 June 2021*

Citation:
Li M, Zhu L, Wang J, Ju J, Liu C, Ma Q, Xu T, Qiao B and Wang X (2021) Holocene Lake Evolution and Glacial Fluctuations Indicated by Carbonate Minerals and Their Isotopic Compositions in the Sediments of a Glacial Melt Recharge Lake on the Northwestern Tibetan Plateau. Front. Earth Sci. 9:656281. doi: 10.3389/feart.2021.656281

HIGHLIGHTS

- Guozha Co has been a closed basin since at least 8.7 kyr BP, based on the high correlation coefficient noted between $\delta^{13}C_{\text{-VPDB}}$ and $\delta^{18}O_{\text{-VPDB}}$ for calcite.
- Climatic change is reflected in the influence of glacial meltwater on the lake water temperature and the oxygen isotopic values.
- Three stages (8.7–4.0, 4.0–1.5, and 1.5 kyr BP to present) can be distinguished based on the decrease in glacial meltwater recharge.
- The lake changed from a fresh lake during 8.7–1.5 kyr BP to a brackish lake from 1.5 kyr BP to present.

INTRODUCTION

Lakes and glaciers are widely distributed on the Tibetan Plateau (TP) (Yao et al., 2019), which is particularly sensitive to climatic changes and is currently experiencing significant warming (Chen et al., 2015). With climate warming, numerous glaciers on the TP are shrinking. These shrinkages have different temporal–spatial features (Yao et al., 2012) and make different contributions to lake expansions (Yang et al., 2017). On the northwestern TP, which is an extremely cold and dry area of the Eurasian continent (Zheng, 1996), the maintenance or expansion of lakes is mainly supported by glacial meltwater under conditions of severely low precipitation (e.g., 61.6 mm/yr) and when there are huge differences between precipitation and evaporation (e.g., 1,361 mm/yr) (Qiao and Zhu, 2019). However, several studies have reported that the glaciers on the northwestern TP are relatively stable, even perform advancing. This so-called Karakoram anomaly (Bolch et al., 2012; Kääb et al., 2012) is contradictory to the expansion of lakes in this area that have mainly been supplied by glacial meltwater in the recent years. Present-day lake water balance studies are important because they reveal the essential relationships between glaciers and lakes. Proxies in ice cores provide detailed climatic records for long geological periods (Thompson, 2000), but they contain less direct indicators of the glacier movement. Moraines are direct relics of glacial movement (Owen and Dortch, 2014), but due to their discontinuities and reformation following their deposition, continuous glacial movements are not well recorded (Xu and Yi, 2017).

The $\delta^{18}O$ and $\delta^{13}C$ values for aragonite and calcite (if autogenous) in lacustrine sediments are controlled by the isotopic composition and temperature of the lake water (Leng and Marshall, 2004; Horton et al., 2016). Thus, calcite and aragonite and their isotopic compositions ($\delta^{18}O$ and $\delta^{13}C$) in lake sediments are widely used to investigate past changes in temperature and the $\delta^{18}O$ of lake water, as well as the paleoenvironmental and paleoclimatic changes (Talbot, 1990; Leng and Marshall, 2004; Henderson et al., 2010; Deocampo and Tactikos, 2010; Hren and Sheldon, 2012; Bernasconi and McKenzie, 2013; Wang et al., 2013; He et al., 2016; and references therein). These proxies may indicate the degree of closure of a lake and may contain signals of glacial meltwater linked with glacier movement. In order to understand how a lake responded to glacier changes, we used a 407-cm-long sediment core to examine the relationship between the glaciers and lake changes. The core was drilled at Guozha Co on the northwestern TP, which is directly supplied by glacial meltwater from the Western Kunlun Mountains.

STUDY AREA

Guozha Co is a semi-closed lake located on the southern slope of the West Kunlun Mountains (**Figures 1A,B**). The lake is surrounded by bedrock slopes with undeveloped lake shore terraces (Li et al., 1991). The bedrock of the lake basin is primarily composed of clastic, metamorphic, and igneous rocks, mainly consisting of conglomerate, sandstone, siltstone, mudstone, limestone, shale, pyroclastic rock, granite, gneiss, diabase, and ophiolite (Bureau of Geology and Mineral resources of Xizang Autonomous Regions, 1993). The lake has an area of 248 km^2 with a maximum depth of 149.5 m and situated at an altitude of 5,080 m above sea level (asl) (Qiao et al., 2017). There are 62 glaciers in the catchment with a total glacier area of 544 km^2 (Li et al., 1993), the meltwater of these glaciers contributed the local hydrology of the lake. When the lake level is high, the lake water flows into Aksai Chin Lake via a channel in the western section (**Figure 1**). As the fresh glacial meltwater enters the lake through rivers in the east and north sections, the present lake's salinity exhibits spatial differences (**Figure 1C**; **Table 1**). Due to the high altitude, the lake region is characterized by cold and thin air with strong solar radiation and large temperature differences (Li et al., 1991; Yao et al., 2013). According to the China Meteorological Forcing Dataset, the mean annual precipitation and mean annual temperature were 90 mm and −12.9°C, respectively, from 1979 to 2013 (Qiao et al., 2017). The observed temperature of the surface water was 4.17°C in September 2015. Due to the low temperature and low amount of precipitation, the lake basin only contains sparsely distributed desert vegetation.

MATERIALS AND METHODS

Li et al. (2021) used the $\delta^{18}O_{\text{carbonate}}$ data from another core (GZHC 2014-1, 304.5-cm long) to quantitatively estimate the Holocene variations in the glacier meltwater in Guozha Co, but they did not discuss the influences of glacial meltwater on the chemical characteristics of the lake water and mineral precipitation in the lake. In addition, core GZHC 2014-1 was collected from a steep underwater slope in the southwestern part of the lake where the lake water is less influenced by the glacial meltwater (**Figure 1C**), and the sediments (including carbonate) are largely controlled by terrestrial debris input.

To more extensively determine the glacial meltwater's influence, using the core sediment and proxy data (carbonate minerals, $\delta^{18}O$ and $\delta^{13}C$, and geochemical characteristics of carbonates), this study is focusing on the evolution of the lake's status and the impact of glacial fluctuation on Guozha Co lake. In 2015, a 407-cm-long sediment core (GZLC15-1, 35°01′8.18″ N, 81°03′37.25″ E; 5,080 m asl; **Figure 1**) was retrieved from the center of Guozha Co using a piston corer.

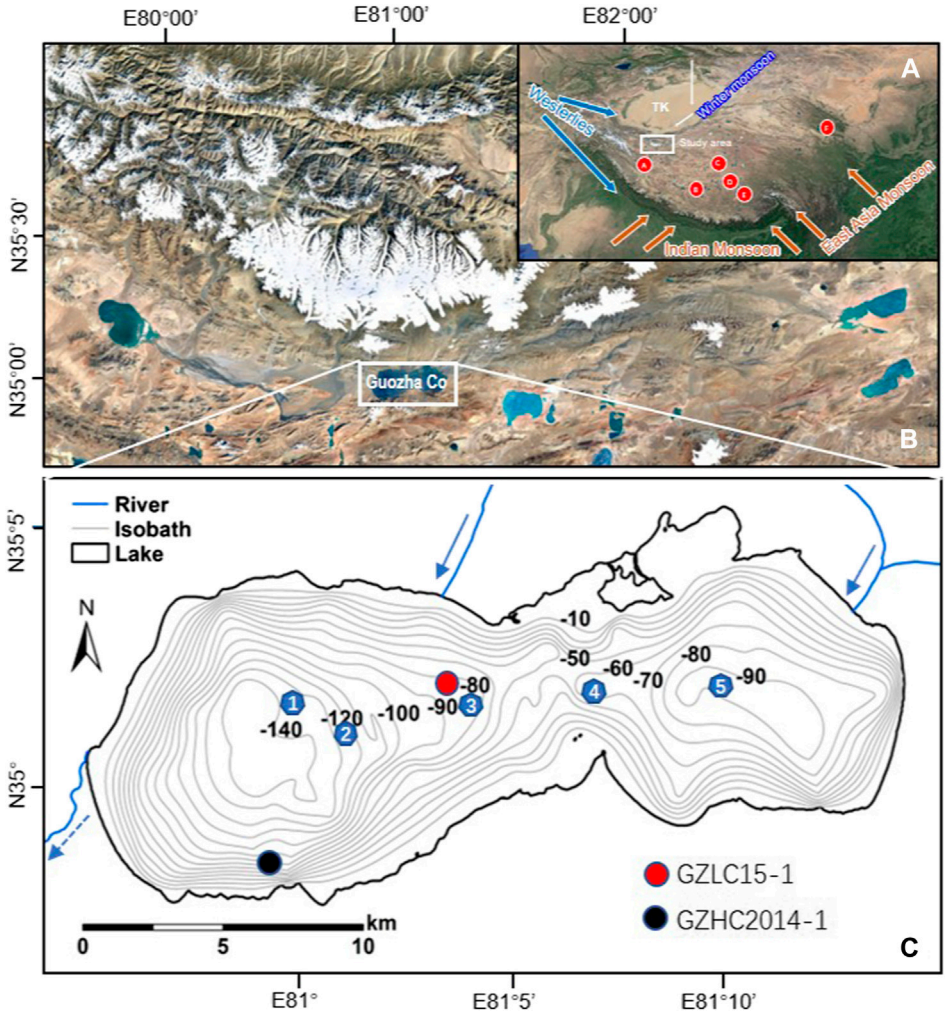

FIGURE 1 | (A) Location of Guozha Co and the other lakes referred to in this study. TK-Taklimakan Desert. A: Bangong Co; B: Taruo Co; C: Buro Co; D: Lingge Co; E: Selin Co; F: Qinghai Lake; **(B)** Relative positions between Guozha Co and glacier; **(C)** Isobath map showing sampling sites of surface lake water(blue number), the cores GZLC15-1, this study and the core GZHC2014-1 by Li et al. (2021).

TABLE 1 | Salinity, pH, ion concentrations (ppm), and temperature (°C) of Guozha Co water

Location	pH	Salinity (g/L)	CO_3^{2-}	HCO_3^-	Cl^-	SO_4^{2-}	Ca^{2+}	Mg^{2+}	K^+	Na^+	Mg/Ca (molar)	Temperature (°C)	References
Center	8.29	3.83	92.26	860	1,348	221	2.57	123	112	1,080	47.9		Li et al. (1993)
Southeast	8.94	2.46	86.49	776	1,180	238	6.51	113.4	96	960	17.5		
Site ①	9.08	3.32										4.34	This study
Site ②	9.11	3.28										4.25	
Site ③	9.08	3.24			1,667	198	19.2	154	82	989	8.02	4.64	
Site ④	9.08	3.19										4.86	
Site ⑤	9.06	3.21										5.03	

The water depth at the drilling site was about 88.3 m. The core contained continuous lacustrine accumulation of silt clay with carbonates. The sediment core was kept intact in the polycarbonate (PC) tube that was used for the core collection while it was transported to the laboratory, where it was sliced at 1-cm intervals. All of the samples were stored at 4–6°C.

Sediment Dating and the Depth–Age Model

The 407-cm-long core was dated using ^{14}C radioactivity. The samples were collected at different depths and each sample was divided into two parts for bulk organic carbon dating (D_{org}) and bulk inorganic carbon dating (D_{in}). A total of 21 effective dates were obtained (**Table 2**). InCal13 software was applied to convert

TABLE 2 | Conventional ^{14}C dating and calibration ages for core GZLC15-1 from Guozha Co

Depth (cm)	D_{org} (con yr BP)	Error	D_{in} (con yr BP)	Error	D_{org} (cal yr BP)	Error	D_{in} (cal yr BP)	Error	Age effect (yr)	Age (cal yr BP)
1	16,500	50	7,870	30	19,892	204	8,679	91	8,744	–65
70	20,620	60	13,640	40	24,828	311	16,450 (reversed)	205		-
110	17,210	50	9,420	-	20,760	188	10,650	-		1,906
150	15,630	40	-	-	18,872	107	-	-		-
180	17,730	50	11,460	30	21,470	240	13,313	89		4,569
260	17,360	60	12,060	30	20,945	234	13,907	133		5,163
310	17,760	50	12,850	40	21,521	232	15,352	193		6,608
335	14,850	40	13,760	40	17,767	168	16,632 (reversed)	238		-
360	16,830	40	13,400	40	20,295	187	16,114	170		7,370
395	15,670	40	13,770	40	18,907	112	16,650	238		7,906
407	17,960	50	12,880	40	21,749	191	15,392 (reversed)	193		-

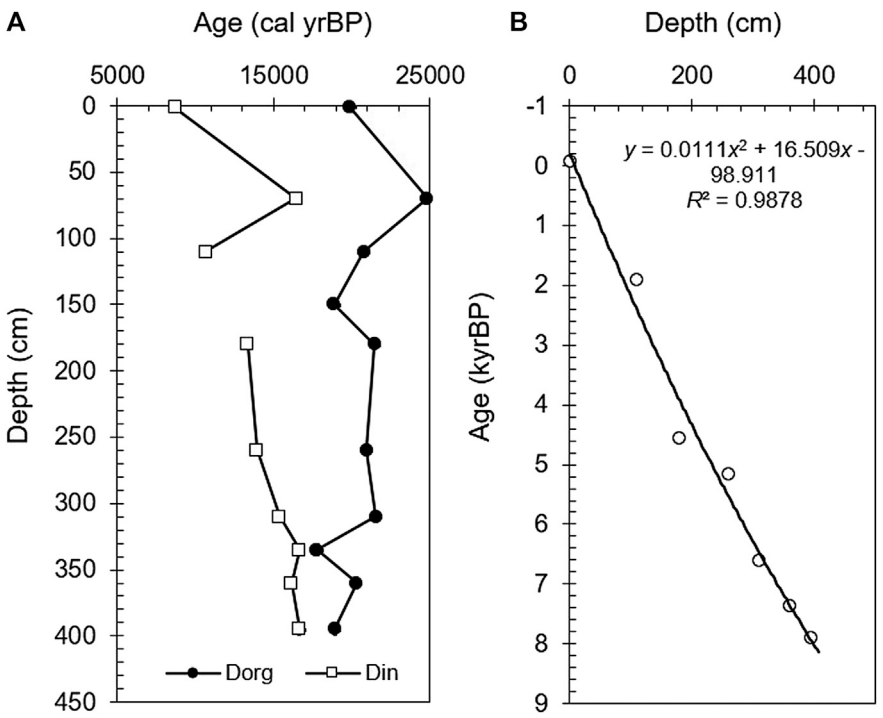

FIGURE 2 | (A) Changes in the bulk organic carbon and inorganic carbon calibrated ^{14}C dates and inorganic carbon age–depth curves with the authigenic carbonate effect removed. **(B)** Diagram of age-depth after removing carbon reservoir effect.

the conventional radiocarbon age to the calendar age (yr BP) (Reimer et al., 2013) and to draw a chrono-depth diagram (**Figure 2A**). The sample analysis was done at the Beta Analytic Radiocarbon Dating Laboratory in the United States.

Environmental Proxies

A total of 44 samples were air dried and ground into fine powder before the various mineral types were identified using an X-ray diffractometer (XRD) (a Rigaku D/MAX-2000, Cu, Kα1, 1.5406 Å, 40 kV, 40 mA, 3–65°, step 0.01°, 10°/min). The minerals were identified by the peak areas. The measurements were conducted at the Micro Structure Analytical Laboratory (MSAL), Peking University, in compliance with the Chinese oil and gas industry standard SY/T 5163-2010.

A total of 82 samples were collected at 5-cm intervals to determine their carbonate Ca and Mg contents. Approximately 0.2 g of each sample was placed in a 15-ml polyethylene centrifuge tube with 10 ml of ultra-pure water to leach the

soluble ions from the pore water. Then, these samples were mixed using a vortex shaker, allowed to stand for 24 h at room temperature, and centrifuged, after which the liquid supernatant was extracted. Then, 10 ml of 1 M acetic acid (HAc) was added, and the samples were allowed to stand at room temperature for 24 h, with occasional shaking. Finally, the solid residues were separated by centrifugation, and the liquid supernatant was collected and analyzed. The Ca and Mg concentrations were determined using inductively coupled plasma optical emission spectroscopy (ICP-OES) at the Institute of Tibetan Plateau Research, Chinese Academy of Sciences (CAS).

A total of 44 bulk sediment samples were selected for carbonate $\delta^{13}C$ and $\delta^{18}O$ analyses, and three of these samples were sieved with a 400-mesh sieve (38-μm mesh) to compare the results of the bulk samples with fine particles. The samples were reacted with 100% phosphoric acid in reaction vessels for at least half an hour at 70°C to liberate the CO_2 gas, and then, the carbon and oxygen isotopes of the CO_2 were analyzed using an IsoPrime100 gas source stable isotope ratio mass spectrometer equipped with a MultiPrep system at the Institute of Earth Environment, CAS. The $\delta^{18}O$ and $\delta^{13}C$ values were normalized to the recommended values for international reference standards NBS-19 and SLAP. All of the $\delta^{18}O$ and $\delta^{13}C$ values have been reported in δ notation relative to Vienna Pee Dee Belemnite (VPDB). The standard results showed that the precision of the $\delta^{18}O_{\text{-VPDB}}$ and $\delta^{13}C_{\text{-VPDB}}$ analysis was better than 0.08 and 0.06‰ (2σ), respectively.

The $\delta^{18}O_{calcite}$ and $\delta^{18}O_{aragonite}$ values were calculated using the following equation (Wang et al., 2008):

$$\delta^{18}O_{\text{bulk carbonate}} = \delta^{18}O_{calcite} \times a + \delta^{18}O_{aragonite} \times b,$$

where a and b are the proportions of calcite and aragonite to the bulk carbonate (a + b = 1), respectively. Generally, the $\delta^{18}O$ of aragonite is about 0.6‰ more positive than that of calcite under the same conditions (Land, 1980; Grossman and Ku, 1986; Abell and Williams, 1989), that is, $\delta^{18}O_{calcite} + 0.6‰ = \delta^{18}O_{aragonite}$.

RESULTS

Sediment Dating

Generally, the bulk organic carbon is a mixture carbon from terrestrial plants, aquatic plants, and topsoil organics. Terrestrial plant carbon is related to the atmospheric CO_2 during plant growth; aquatic plant carbon utilizes the CO_2 dissolved in the water; and the topsoil organic carbon is related to the soil formation process. The atmospheric CO_2 is generally constant. The CO_2 in the water comes from the atmospheric CO_2 and is also released from clastic carbonates during their dissolution.

Terrestrial plant carbon comes from the assimilation of atmospheric CO_2 during the growth process, and exhibits obvious decay after a long period of burial. The relatively stable dating data for the bulk organic carbon from the bottom to the top of the GZLC15-1 core indicate that terrestrial organic carbon contributed less to the bulk organic carbon dating. In the arid/cold climatic condition, the soil formation processes are weak, resulting in less supply of topsoil organic carbon. Therefore, the bulk organic carbon dating data (D_{org}) of the GZLC15-1 core should be predominately influenced by the aquatic plant carbon. However, aquatic plants that used dissolved CO_2 in the water also did not change the stability of the bulk organic carbon dating data from the bottom to the top of the core. This indicates that the dissolved CO_2 in the lake water, although used by aquatic plants found at different burial depths (different burial times), was from the same period and less influenced by atmospheric CO_2 of the sedimentary period. In particular, the oldest date was around 20,000 years BP, which coincides with the Last Glacial Maximum (LGM), implying that CO_2 that was frozen and trapped in the glaciers during the LGM came into the lake with glacial meltwater.

The ^{14}C ages of the bulk organic carbon did not increase with depth. Therefore, the ^{14}C dates of the inorganic carbon, which are also related to the CO_2 dissolved in the lake, were considered when constructing the age sequence. As can be seen from **Figure 2A**, the inorganic carbon dates (D_{in}) gradually decrease from bottom to top, indicating that a rational sequence exists between the inorganic carbon dates (D_{in}) and the depositional depth. The inorganic carbon in the lake sediments is a mixture of authigenic carbonate and clastic carbonate. As the isotopes of fine-grained (<38 μm) carbonates are similar to those of the bulk carbonate, the bulk carbonate is concluded to be authigenic (see section "Origin of carbonate minerals and $\delta^{18}O_{\text{-VPDB}}$ and $\delta^{13}C_{\text{-VPDB}}$") based on the balance of Ca^{2+} in the equation $2HCO_3^- = CaCO_3 + CO_2 + H_2O$. Fontes et al. (1996) discussed the formation of lake authigenic calcite in Bangong Co, which is located in the same area as Guozha Co, and concluded that the authigenic calcite was mostly formed under the influence of dissolved carbonate from the basin's surface soil and the CO_2 released from deep fractures in the fault zones. It was further concluded that the CO_2 released from the deep fracture in the fault zones was roughly similar to the atmospheric CO_2 at the time. However, despite the extreme drought in the Guozha Co basin, the limited surface water produced by precipitation can still form carbonates in the surface soil, and thus, the surface soil contains atmospheric CO_2 information. After the carbonates in the surface soil are transported into the lake by the glacial meltwater, groundwater, and atmospheric precipitation, the carbon isotopes of these carbonates reflect the characteristics of the atmospheric CO_2 during its deposition into the lake. The deposition age can be obtained if the authigenic carbonate age effect (only using water CO_2) is removed from the inorganic carbon age results.

As we do not know the ratio of the surface soil carbonate to the lake water authigenic carbonate, it is simply assumed that the difference between the calendar age of the top layer of inorganic carbon and its actual age (1 year before sampling) is the age effect. Thus, the age effect can be eliminated by subtracting the age effect from the bulk inorganic carbon age of each depth. Based on this calculation, we constructed an age sequence for the entire core and plotted the core's depth–age curve (**Figure 2B**). The correlation between age and depth was obtained via quadratic multiphase fitting of the data, and the age corresponding to each depth was calculated.

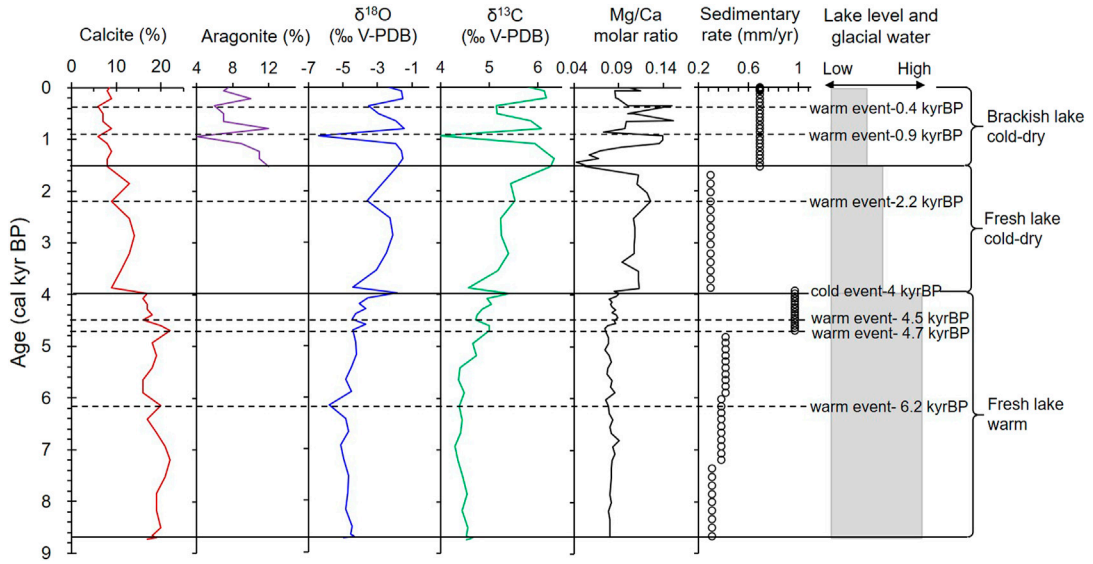

FIGURE 3 | Overview of the ages and multiple proxies for core GZLC15-1, showing the changes in the sedimentary environment and climate since 8.7 kyr BP.

Mineralogical Features

Two types of carbonate minerals were identified using X-ray diffraction. Calcite is the main carbonate phase, and it is continuous in the core with contents of 6–22% (average 14.5%; **Figure 3**). However, the aragonite is only present in the top part of the core (0–110 cm; until 1.5 kyr BP), and ranges between 4% and 12%. The minimum concentration (4%) of aragonite is observed at around 0.9 kyr BP. The $MgCO_3$ concentration of the calcite is less than 1%, indicating that it is low-Mg calcite. The calcite content shifts dramatically at a depth of 190 cm (4.0 kyr BP), after which it exhibits a decreasing trend. Dolomite is a minor component, accounting for less than 5% (**Table 3**).

Geochemistry, $\delta^{18}O_{\text{-VPDB}}$ and $\delta^{13}C_{\text{-VPDB}}$

Calcium is the main element in carbonate minerals, and the Ca content of the core ranges between 39.1 and 148.4 mg/g. Mg and Sr are minor elements that enter the carbonate mineral lattice to replace Ca, and their contents are 2.8–8.9 mg/g and 0.16–2.16 mg/g, respectively. Ca and Mg have similar curves at 8.7–4.0 kyr BP, and Ca and Sr have similar curves after 1.5 kyr BP. The Mg/Ca molar ratios are less than 0.16 (**Figure 4**). The K and Na curves are similar to those of Ca, Mg, and Sr after 4.0 kyr BP. The Na content increases with decreasing depth. Peaks in the element concentrations occur at 6.7, 6.2, 4.5, and 2.2 kyr BP, but they are not always consistent with those of the carbonate minerals (**Figure 4**).

At depths of 407–110 cm (8.7–1.5 kyr BP), calcite is the only carbonate mineral. The $\delta^{18}O_{calcite}$ values range from −5.79‰ to −1.87‰, while the $\delta^{13}C_{calcite}$ values range from 5.53‰ to 4.36‰. Little change was noted in the $\delta^{18}O_{\text{-VPDB}}$ and $\delta^{13}C_{\text{-VPDB}}$ values during 8.7–4.0 kyr BP, but the values of both distinctly increased during 4.0–1.5 kyr BP. After 1.5 kyr BP, the carbonate minerals consisted of calcite and aragonite. The $\delta^{18}O_{calcite+aragonite}$ values ranged from −6.39‰ to −1.43‰, while the $\delta^{13}C_{calcite+aragonite}$ values ranged from 3.98 to 6.34‰. The values of both $\delta^{18}O_{\text{-VPDB}}$ and $\delta^{13}C_{\text{-VPDB}}$ increased gradually and then shift dramatically from 4.0 to 0.9 kyr BP (**Figure 3**).

DISCUSSION

Origin of Carbonate Minerals and $\delta^{18}O_{\text{-VPDB}}$ and $\delta^{13}C_{\text{-VPDB}}$

Regardless of the lake water type, the first minerals to precipitate from water are alkaline earth carbonates, and their sequence is calcite followed by argonite and then dolomite. These carbonate minerals are also formed by the diagenetic action of the pore water during postdepositional processes and even during syn-depositional diagenesis (Hardie et al., 1985; Warren, 1989). As the pore water is basically captured lake water, it is impossible to distinguish between the authigenic and endogenic carbonates.

Lacustrine aragonite is authigenic and/or endogenic because it is a metastable mineral and is never found in ancient carbonate rocks. Lacustrine aragonite is generally found in saline or brackish lakes (Fontes et al., 1996; Digerfeldt et al., 2000; Landmanna et al., 2002; Shapley et al., 2005; Murphy et al., 2014). In the process of seawater evaporation, aragonite begins to precipitate when the solution reaches 2–3 times the concentration of seawater (Warren, 1989). Therefore, the presence of aragonite generally suggests that the lake water was brackish during the depositional period. In the core, aragonite is only present in the upper 110 cm (1.5 kyr BP), with a content of less than 12% (**Table 3**). This indicates that the Guozha Co water became brackish at least 1.5 kyr BP ago according to the classification of lakes based on salinity (fresh lake: salinity <1 g/L; brackish: 1–35 g/L; saline lake: 35–50 g/L; salt/salar lake: >50 g/L; Zheng et al., 2002).

TABLE 3 | Mineral content (%) and isotopic composition (‰VPDB)

Depth (cm)	Calcite	Aragonite	Dolomite	δ^{18}O-bulk	δ^{13}C-bulk	δ^{18}O-calcite	δ^{18}O-aragonite
1	9	8	3	–2.92	5.51	–3.20	–2.60
10	8	7	5	–1.61	6.13	–1.89	–1.29
20	9	10	4	–1.54	6.18	–1.86	–1.26
30	6	6	3	–3.53	5.15	–3.83	–3.23
40	7	7	4	–2.94	5.16	–3.24	–2.64
50	7	7	4	–1.95	5.86	–2.25	–1.65
60	9	12	3	–1.43	6.08	–1.77	–1.17
70	6	4	3	–6.39	3.98	–6.63	–6.03
80	8	9	4	–1.92	5.94	–2.24	–1.64
90	9	11	3	–1.59	6.15	–1.92	–1.32
100	8	11	4	–1.52	6.34	–1.87	–1.27
110	8	12	4	–1.80	6.26	–2.16	–1.56
120	13		4	–2.73	5.44	––2.73	
130	9		3	–3.60	5.53	–3.6	
140	13		2	–2.26	5.23	–2.26	
150	14		3	–2.12	5.25	–2.12	
160	13		4	–2.48	5.40	–2.48	
170	11		4	–3.05	5.17	–3.05	
180	9		3	–4.41	4.57	-4.41	
190	17		3	–1.87	5.41	–1.87	
200	16		3	–3.55	4.96	–3.55	
210	17		3	–4.05	5.05	–4.05	
220	17		3	–3.66	4.85	–3.66	
230	18		5	–4.27	4.75	–4.27	
240	16		3	–4.48	4.72	–4.48	
250	20		3	–3.69	5.00	–3.69	
260	22		3	–4.41	5.00	–4.41	
270	18		4	–4.26	4.67	-4.26	
280	19		4	–4.21	4.73	–4.21	
290	18		4	–4.51	4.40	–4.51	
300	16		3	–4.82	4.37	–4.82	
310	16		3	–4.51	4.49	–4.51	
320	20		4	–5.79	4.38	–5.79	
330	17		3	–4.85	4.45	–4.85	
340	19		4	–4.69	4.41	–4.69	
350	21		4	–5.12	4.29	–5.12	
360	22		3	–4.95	4.36	–4.95	
370	21		4	–4.65	4.46	–4.65	
380	19		3	–4.72	4.54	–4.72	
390	19		3	–4.83	4.45	–4.83	
400	20		3	–4.47	4.56	–4.47	
405	18		3	–4.54	4.53	-4.54	
406	19		3	–4.34	4.66	–4.34	
407	17		4	–4.95	4.53	–4.95	

Dolomite is common in ancient carbonates and is rare in Holocene sediments. As it is an evaporative mineral, laboratory experiments have shown that it is not able to precipitate in fresh water at Earth surface temperatures without bacterial mediation (Warren, 2000). It is very likely that the dolomite present in the section of the core deposited during the fresh water stage, that is, from the bottom (8.7 kyr BP) to 110 cm (1.5 kyr BP), was detrital and was transported by water from the surrounding catchment, most likely from the adjacent TK desert. Since the dolomite concentration was <5% in the core sediment, the bulk carbonates composition are dominantly controlled by the calcite.

At high altitudes, the wind contribution to sediments can usually not be ignored. In the Guozha Co sediments, the fine grain size (less than 38 μm) is dominant (Li et al., 2021), while the <75 μm fraction from the Chinese desert is less than 8% (Rao et al., 2009). This indicates that the amount of fine grains from the adjacent TK desert may be very small or trace, and the detrital sediments in Guozha Co are mainly from the local weathering of rocks and were transported by river water and wind.

There are three hypotheses regarding the formation of calcite: (1) chemical precipitation; (2) detrital sources; and (3) biological origin (Fontes et al., 1996; Digerfeldt et al., 2000; Landmanna et al., 2002; Shapley et al., 2005; Liu et al., 2009; Murphy et al., 2014; McCormack et al., 2019). The amount of calcite debris mainly depends on the chemical weathering and wind contribution. In the dry and cold climate of the Guozha Co area, the mean annual precipitation and temperature from 1979 to 2013 were 90 mm and −12.9°C, respectively (Qiao et al., 2017), which suggests that the intensity of chemical weathering in the

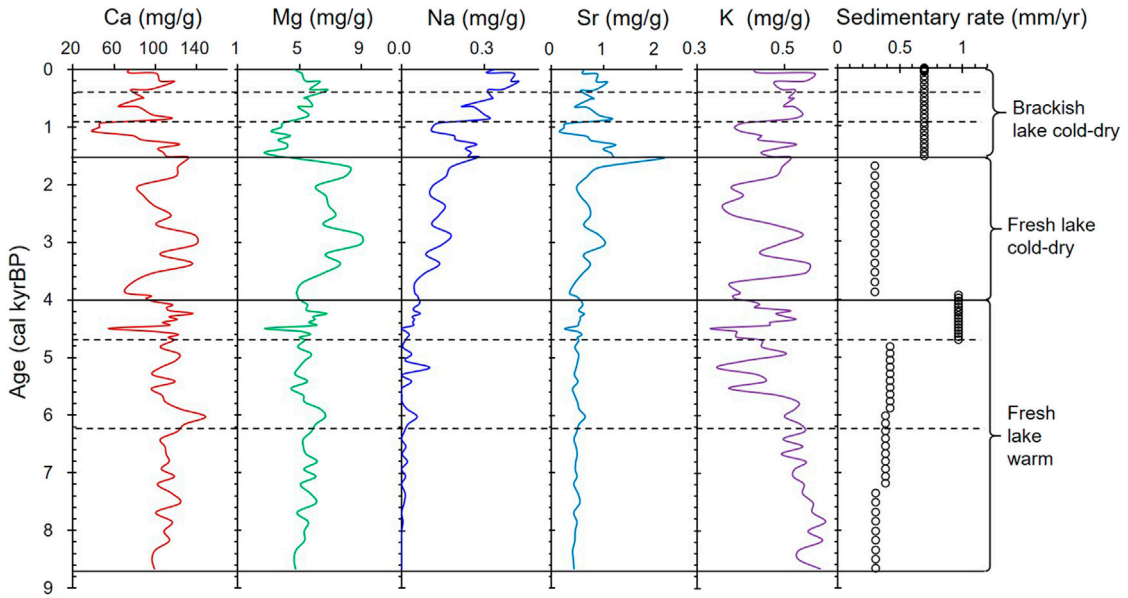

FIGURE 4 | Plot of ion content versus age showing the changes in the sedimentary environment and climate since 8.7 kyr BP.

TABLE 4 | Isotopic comparisons of bulk and fine-grained carbonates (‰VPDB)

Depth (cm)	Calcite in bulk	Aragonite in bulk	δ^{18}O-bulk	δ^{13}C-bulk	δ^{18}O-fine grain	δ^{13}C-fine grain	$\Delta\ \delta^{18}O_{(\text{fine grain-bulk})}$
70	6	4	−6.39	3.98	−4.82	4.69	1.57
150	14		−2.12	5.25	−1.63	5.49	0.49
330	17		−4.85	4.45	−4.25	4.9	0.6

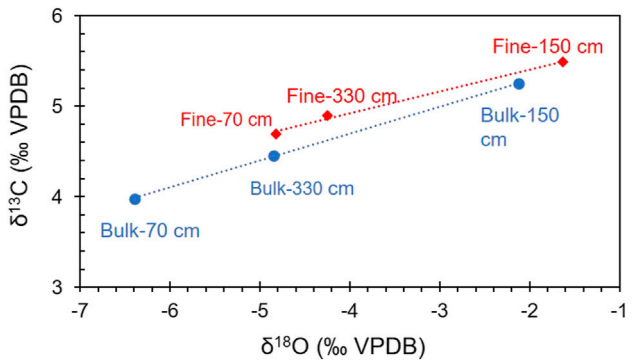

FIGURE 5 | Comparison of the δ^{18}O (‰VPDB) and δ^{13}C (‰VPDB) values of the fine-grained and bulk carbonates in core GZLC15-1 from Guozha Co.

lake basin was very weak and thus the clastic calcite content of the lake sediments should be low.

Biological shells such as ostracod shells normally weigh only a few micrograms and are only a minor component of lacustrine sediments (Liu et al., 2009; McCormack et al., 2019). Therefore, most of the calcite in the lake sediments must have been produced by chemical precipitation, and the bulk carbonate is mainly authigenic.

The isotopic composition of the bulk carbonate in the upper 110 cm may contain a contribution from both aragonite and calcite, while only calcite contributes to the isotopic composition of the bulk carbonate at depths of 110–407 cm. Although the $\delta^{18}O\text{-}_{VPDB}$ and $\delta^{13}C\text{-}_{VPDB}$ values of the calcite may contain contributions from chemical, minor detrital, and biological (mainly ostracods) calcite in the core, the detrital carbonate and the "vital offsets" from the ostracods have little influence on the isotopic composition of bulk calcite in cold–dry regions. This is due to the following reasons: 1) The δ^{18}O values of calcite with a biological origin, such as ostracod shells, are close to those of inorganic calcite, and they mainly reflect the isotopic variations of the water in the lake sediments, with a mean offset of +1.3‰ (Liu et al., 2009; Guo et al., 2016; Börner et al., 2017). Thus, the "vital offsets" from ostracods have little influence on the oxygen isotopes of bulk carbonate as they only weigh a few micrograms; and 2) the δ^{18}O values of the fine-grained carbonate (considered to be authigenic) in this study are close to those of the bulk carbonate and the correlation between $\delta^{18}O\text{-}_{VPDB}$ and $\delta^{13}C\text{-}_{VPDB}$ is linear (**Table 4**; **Figures 5**, **6**). The $\delta^{18}O\text{-}_{VPDB}$ values of the fine-grained carbonate are only 0.49‰, 0.6‰, and 1.57‰ more positive than the bulk carbonate values at depths of 330, 150,

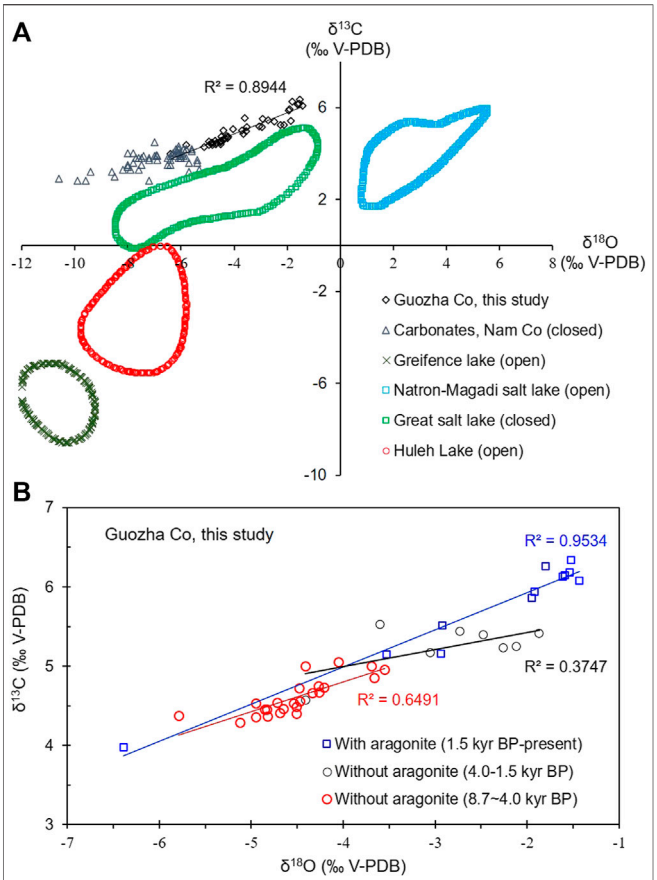

FIGURE 6 | Comparison of the $\delta^{18}O$ (‰VPDB) and $\delta^{13}C$ (‰VPDB) values from **(A)** Guozha Co and other lakes **(B)** from different stages in Guozha Co. The $\delta^{18}O$ and $\delta^{13}C$ data for Nam Co are from Li et al. (2012), and the data for the other lakes are from Talbot (1990).

and 70 cm, respectively (**Table 4**). The most positive value of 1.57‰ at a depth of 70 cm is due to the presence of aragonite because under the same conditions, the $\delta^{18}O$ of aragonite is about 0.6‰ more positive than that of calcite (Land, 1980; Grossman and Ku, 1986; Abell and Williams, 1989). These facts suggest that the isotopic compositions of the bulk and fine-grained carbonate were both controlled by the isotopic composition of the lake water. However, not all fine-grained carbonates are authigenic/endogenic. This is why many studies have used the isotopic composition of the bulk carbonate to trace paleoenvironmental changes in lakes (Keatings et al., 2002; Liu et al., 2009; Wünnemann et al., 2018; McCormack et al., 2019).

The $\delta^{18}O_{carbonate}$ is dependent on the oxygen isotopic composition of the water ($\delta^{18}O_{water}$) and the temperature at which the carbonate minerals formed. It is a function of water temperature (T_{water}) and follows the temperature-dependent fractionation equation: T_{water} (°C) = 13.8–4.58 × ($\delta^{18}O_{carbonate} - \delta^{18}O_{water}$) + 0.08 × ($\delta^{18}O_{carbonate} - \delta^{18}O_{water}$)^2 (Kim and O'Neil, 1997; Leng and Marshall, 2004). The influence of dolomite on the $\delta^{18}O_{carbonate}$ values can be ignored because CO_2 is generally released from dolomite at 90°C, but in this study, the $\delta^{18}O_{carbonate}$ was examined at 70°C. In the upper 110 cm, the $\delta^{18}O_{carbonate}$ values resulted from the mixing of the calcite and aragonite oxygen isotopic compositions. The fractionation factors of the inorganic calcite $\alpha_{calcite\text{-}water}$ and aragonite $\alpha_{aragonite\text{-}water}$ values are different, and under the same conditions, $\delta^{18}O_{aragonite}$ is enriched relative to $\delta^{18}O_{calcite}$ (Land, 1980; Grossman and Ku, 1986; Abell and Williams, 1989). Regardless of their fractionation factors, both the $\delta^{18}O_{calcite}$ and $\delta^{18}O_{aragonite}$ values are dependent upon the $\delta^{18}O_{water}$ and the T_{water}. A high T_{water} under warm conditions contributes to a high $\delta^{18}O_{carbonate}$ (i.e., ^{18}O enrichment). However, the recharge of glacial meltwater with very negative $\delta^{18}O$ values and a low temperature can decrease the temperature of the lake water and the $\delta^{18}O_{lake\ water}$ and $\delta^{18}O_{carbonate}$ values at the same time. Glacial melting occurs under warm climate conditions. As Guozha Co is a glacial melt recharge lake, the low $\delta^{18}O_{carbonate}$ values of core GZLC15-1 may represent a large amount of recharge by glacial water and a warm climate. This is further supported by the presence of similar trends in the $\delta^{18}O_{carbonate}$ of core GZLC15-1 and the $\delta^{18}O$ of an ice core (**Figure 7**) from the Guliya Ice Cape, the glacial meltwater of which directly supplies Guozha Co (**Figure 1**).

The $\delta^{18}O$ of glacial meltwater is also a sensitive proxy for temperature and climatic change (Yao et al., 2013; Yu et al., 2016; Thompson et al., 2018), and it is very negative compared with $\delta^{18}O_{carbonate}$ in lacustrine sediments. In addition to temperature, the latter is mainly controlled by the ratio of the water input to output, that is, evaporation and precipitation plus glacial meltwater. Consequently, the $\delta^{18}O_{carbonate}$ oscillations in core GZLC15-1 are not always consistent with the $\delta^{18}O$ records of the Guliya ice core (**Figure 7**).

Carbonate Elements and Glacial Effects

The chemical components of the lake water are the most crucial factors controlling the authigenic and/or endogenic carbonate mineral precipitation. A dry climate will increase the soluble ion concentrations in lake water, while glacial meltwater will reduce the soluble ion concentrations. Ca is the main element in carbonates, and it has an ionic radius similar to the ionic radii of Mg and Sr. Due to the different crystal structures of calcite and aragonite, the Ca in calcite is often replaced by Mg and Sr, while the Ca in aragonite is often replaced by Sr. This is why the correlation coefficients between Ca and Sr are high throughout the core, while a high coefficient between Ca and Mg is only evident during 8.7–1.5 kyr BP (**Figure 8**) when calcite was the dominant carbonate mineral, and there was no aragonite. In the inorganic precipitation of carbonates, when the Mg concentration in the lake water becomes high, calcite formation is inhibited and aragonite precipitation increases (Shapley et al., 2005; Rivadeneyra et al., 2006; Li et al., 2009). Thus, the correlation coefficient between Ca and Mg decreased from 8.7 to 4.0 kyr BP (R^2 = 0.8607) to 4.0–1.5 kyr BP (R^2 = 0.7703) and from 1.5 kyr BP to present (R^2 = 0.0149; **Figure 8**). This may be due to the increasing Mg concentration in the lake water as well as the presence of both calcite and aragonite during the last stage. These effects resulted from a dry climate and the reduced recharge from glacial meltwater.

Similarly, the changes noted in the correlation coefficient between Ca and Na (**Figure 8**) indicate that the Na content is related to the calcite content in the core. Unlike Mg and Sr, Na is

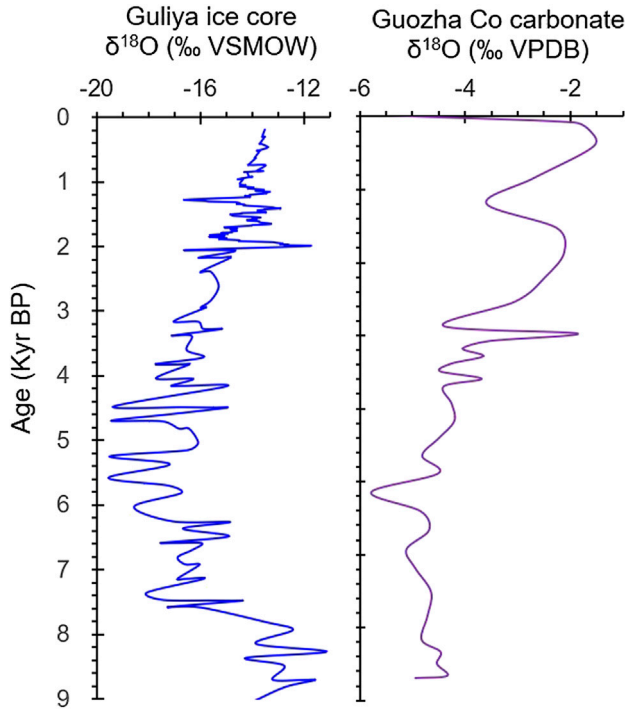

FIGURE 7 | Comparison of the oxygen isotopic compositions of the carbonates in core GZLC15-1 and the Guliya ice core. The $\delta^{18}O$ data for the ice core are from Yang et al. (2006) and Thompson et al. (2018).

more sensitive to changes in salinity. The increasing Na content indicates that the climate gradually became dry, and the recharge from glacial meltwater gradually decreased after 8.7 kyr BP. The Na content was very low (even zero) during 8.7–4.0 kyr BP (**Figure 4**), which may be due to the glacial meltwater. During this period, the correlation coefficient between Ca and K was also low and similar to that between Ca and Na. This indicates that K content was also mainly related to the calcite content. However, the K and Na curves depict different trends, and the K content is higher than the Na content (**Figure 4**). It is well known that in nature, the K content of water is lower than that of Na. It is difficult to judge the effect of climate and glacial meltwater on the K content of carbonates and lake water. One possible reason for this is that some of the K came from the acid dissolution of clay minerals, although we used acetic acid (HAc, weak acid).

Lake Status and Glacial Effects

Guozha Co has been a closed basin since at least 8.7 kyr BP, based on the high correlation coefficient noted between $\delta^{18}O$-$_{VPDB}$ and $\delta^{13}C$-$_{VPDB}$ values ($R^2 = 0.89$; **Figure 6**). In the $\delta^{18}O$–$\delta^{13}C$ plot, all of the data are distributed within the same quadrant, as similar to other closed lakes, such as Nam Co and Great Salt Lake (**Figure 6A**). In general, the relation between $\delta^{18}O$ and $\delta^{13}C$ show weak/insignificant correlation for the carbonates in open lakes, whereas in the closed basins, it shows a strong correlation (Talbot, 1990; Liu et al., 2001). This is because, the water in open lakes flows rapidly and has a short residence time, and as a result, the $\delta^{18}O$-$_{VPDB}$ and $\delta^{13}C$-$_{VPDB}$ values of the lake water reflect the isotopic characteristics of the inflowing water, including meltwater, groundwater and rain water, which are affected by different factors. However, in closed lakes, the residence time of the water is long, and evaporation plays a controlling role in the lake water's composition. Moreover, closed lakes contain large amounts of algae, which preferentially absorb lighter carbon, resulting in enriched $\delta^{13}C$ values (Kelts, 1988).

As Guozha Co is directly recharged by glacial meltwater, the glacial recharge influenced not only the $\delta^{18}O$-$_{VPDB}$ and $\delta^{13}C$-$_{VPDB}$ values of the calcite and aragonite minerals but also influence the lake level changes. The increase of glacial meltwater will reduce the $\delta^{18}O$ values of carbonate minerals and cause the lake level to rise. According to the variations in the carbonate minerals and the coefficients between $\delta^{18}O$-$_{VPDB}$ and the calcite content and between $\delta^{18}O$ and $\delta^{13}C$, the lake level was highest during 8.7–4.0 kyr BP and lowest from 1.5 kyr BP to present. As most of the calcite was inorganically precipitated from the lake water, in general, the changes in the calcite content and $\delta^{18}O$-$_{VPDB}$ values should be consistent (Li et al., 2008,2012; Liu et al., 2009; McCormack et al., 2019). However, there is no correlation between calcite content and $\delta^{18}O$-$_{VPDB}$ values during 8.7–4.0 kyr BP ($R^2 = 0.1$), whereas the correlation has a high coefficient during 4.0–1.5 kyr BP ($R^2 = 0.85$) and from 1.5 kyr BP to present ($R^2 = 0.51$; **Figure 9**). One possible reason for this is that the inflow of glacial meltwater, which had more negative $\delta^{18}O$-$_{VPDB}$ values than the lake water, was much higher during 8.7–4.0 kyr BP and from 4.0 kyr BP to present. The inflow of fresh meltwater is also supported by the low Na and high Ca

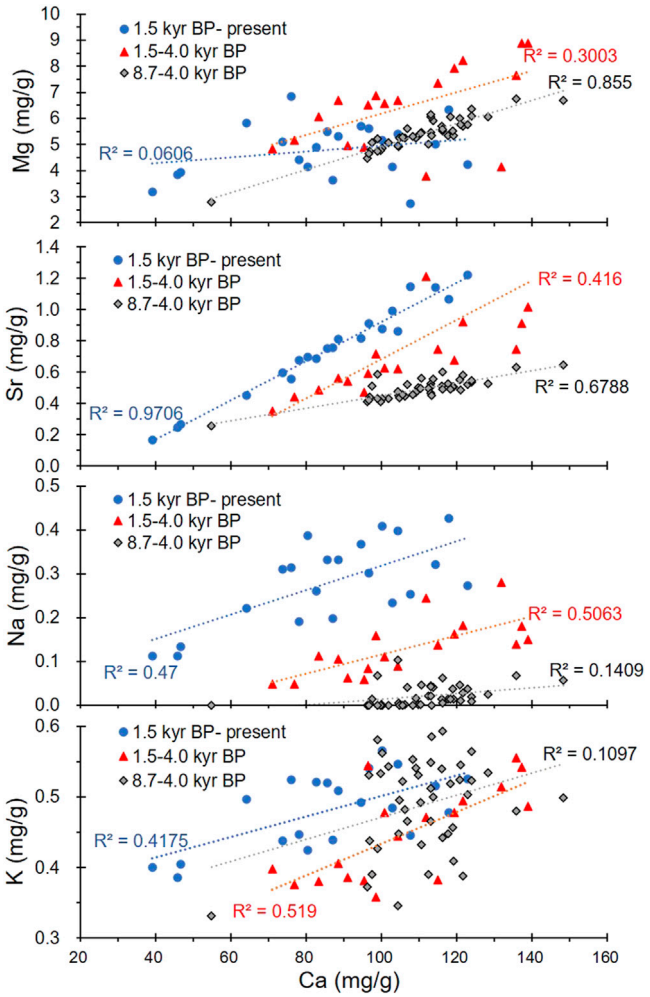

FIGURE 8 | Correlations between the Ca and Mg, Sr, Na, and K contents of the carbonates.

and Mg contents during 8.7–4.0 kyr BP (**Figure 4**). Owing to the very low rainfall and high evaporation in the study area (Qiao et al., 2017), the glacial meltwater is the main input to the lake, and the glacial recharge contributed to the lake level being highest during 8.7–4.0 kyr BP, as indicated by the core data (**Figure 3**).

The lake water level was lowest from 1.5 kyr BP to present based on the presence of aragonite, which is generally precipitated in brackish or saline lake water. The high Na content (**Figure 4**) and the high correlation coefficient between $\delta^{18}O\text{-}_{VPDB}$ and $\delta^{13}C\text{-}_{VPDB}$ (R^2 = 0.95; **Figure 6B**) from 1.5 kyr BP to present also suggest high evaporation, increasing lake water salinity, and a low water level with less glacial recharge (**Figure 3**). Therefore, the recharge from glacial meltwater in the aragonite stage (1.5 kyr BP to present) was less than in the calcite stage (8.7–1.5 kyr BP).

Climatic Change and Glacial Effect

The changes in the mineral composition and element contents of the sediment indicate that the lake water has gradually become more concentrated since 8.7 kyr BP. Three distinct stages can be identified, 8.7–4.0, 4.0–1.5, and from 1.5 kyr BP to present (**Figure 10**), which indicate that the recharge from glacial meltwater has continuously decreased.

Stage I (8.7–4.0 kyr BP): The climate was warm, which is consistent with the Holocene warm optimum and the high global temperature (**Figure 11**). The warm climate during this period has also been indicated by a variety of other land- and marine-based proxy data from all around the world (Marcott et al., 2013). Under these warmer conditions, the glaciers in the West Kunlun Mountains retreated, as corroborated by the $\delta^{18}O$ of ice core water and other climatic proxies (Li, 1996; Thompson et al., 1997; Pang et al., 2020). As a result, the lake's water level rose (**Figure 10**) and the lake water was fresh with low Na content (**Figure 3**). This suggests that the regional glacier was affected by the Holocene climate change, and the $T_{lake\ water}$ was mainly controlled by climate change and not glacial meltwater. The surface lake water temperature results for Guozha Co also support this conclusion. The water temperature in the eastern part of the basin was higher than in the western part of the basin (**Table 1**), despite the fact that the glacial meltwater entered the

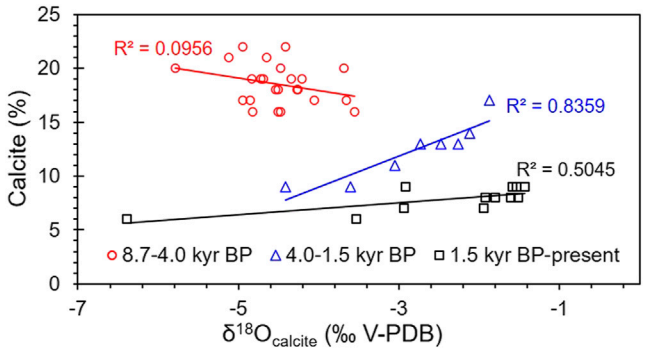

FIGURE 9 | Relationships between the calcite content and $\delta^{18}O_{calcite}$ (‰VPDB) during the different periods.

lake through the eastern part due to the direction of the blowing wind from west to east.

The low $\delta^{18}O$-$_{VPDB}$ values and the slight increasing contents of Ca, Mg, and Na at around 6.2 kyr BP (**Figures 3**, **4**) were also due to climatic change. The warm event at 6.2 kyr BP has also been identified in cores and paleoshorelines from the glacial recharge lakes on the TP, such as Nam Co (at around 6 kyr BP), Lingge Co (~6.1 kyr BP), and Bangong Co (around 6.3–6.0 kyr BP) (Frontes et al., 1996; Gasse et al., 1996; Zhu et al., 2008; Pan et al., 2012). Based on the abrupt increases in the sedimentary rates and high carbonate Mg/Ca molar ratios, there may have been a warm-dry event at 4.7 kyr BP (**Figure 3**). The event at 4.7 kyr BP has also been identified in a core from Ahung Co, a lake in central Tibet (Morrill et al., 2006).

Stage II (4.0–1.5 kyr BP): The climate was cold-dry, which is consistent with the decreasing global temperature (**Figure 10**). The cold climate during this time is well reflected by the famous "4.2 kyr cold event", which is considered to have marked the end of the Holocene warm optimum (Bond et al., 1997; 2001; Xiao et al., 2019; Mehrotra et al., 2019). This cold event has also been recorded in other lake sediments on the TP, such as the fresh-brackish Bangong Co in west Kunlun on the western TP (**Figure 11**) based on the $\delta^{18}O$, $\delta^{13}C$, geochemistry, and grains (Gasse et al., 1996; Wei and Gasse, 1999); Selin Co, a glacial recharge lake on the central TP (**Figure 11**) based on the $\delta^{18}O$ and $\delta^{13}C$ (Gu et al., 1993) and shorelines (Shi et al., 2017); and Qinghai Lake on the eastern TP based on the $\delta^{18}O$ and $\delta^{13}C$ of carbonates (Liu et al., 2003). This event was also observed in other places in the world, such as the Indo-Gangetic Plain (dominated by Indian Summer Monsoon [ISM]) based on the fluvial landscapes (MacDonald, 2011; Giosan et al., 2012), and the PT Tso Lake, Eastern Himalaya (dominated by ISM), based on pollen and carbon isotopes (Mehrotra et al., 2019). The reconstructed sea surface temperatures (SSTs) in the western Bay of Bengal (dominated by ISM) also start to cool off during this stage based on the $\delta^{18}O$ and Mg/Ca ratio of planktonic foraminifera (Govil and Naidu, 2011; **Figure 11**).

Under these cold conditions, the glaciers in the West Kunlun Mountains stopped retreating after 3 kyr BP, which is supported by the ^{10}Be ages of the moraines (Li, 1996; Pang et al., 2020; Chen et al., 2020) and proxies from ice cores (Thompson et al., 1997; Pang et al., 2020). Glacier advances also occurred frequently in the North Atlantic at 4.4–4.2, 3.8–3.4, 3.3–2.8, 2.6, and 2.3–2.1 kyr BP (Solomina et al., 2015). As a result, less meltwater entered Guozha Co and the lake level decreased (**Figure 10**). Although the lake water may still have been fresh, the increased Na content indicates that the lake water became more concentrated (**Figure 4**). Decreasing rainfall was observed in northern Australia (dominated by Australia–Indian summer monsoon [AISM]) during 4.1–1.5 kyr BP based on the $\delta^{18}O$ of stalagmite from Western Australia (Denniston et al., 2013) and southern China (Yuan et al., 2004), and the Ti/Ca ratio of bulk lacustrine sediments in the Lombok Basin in Indonesia (Steinke et al., 2014; **Figure 11**).

Similar to Stage I, the low $T_{lake\ water}$ in Stage II was controlled by the cold climate. The low $T_{lake\ water}$ and the cold climate (e.g., low precipitation/evaporation) driving the hydrochemical conditions (e.g., Mg/Ca ratio) influenced both the calcite precipitation and the $\delta^{18}O$ of the lake water. Thus, the coefficient between the calcite content and the $\delta^{18}O$-$_{VPDB}$ values was high (R^2 = 0.85; **Figure 9**).

In addition to the 4.0 kyr BP cold event, warm events also occurred at 3.9 and 2.2 kyr BP under arid-cold conditions (**Figure 3**). The 2.2 kyr BP event has also been identified in the Nam Co core based on rare earth element concentrations (Li et al., 2011). The 3.9 kyr BP warm event was coincident with a pronounced dry period at Nam Co around 3.7 kyr BP (Mügler et al., 2010), and at Lake Qinghai around 3.9 kyr BP (Shen et al., 2005).

Stage III: From 1.5 kyr BP to present, the climate was basically dry-cold and fluctuated, with two warm events at 0.9 and 0.4 kyr BP in the Guozha Co area (**Figure 3**). During this period, the global temperature also exhibited a decreasing and fluctuating trend (**Figure 11**). The deterioration and fluctuations in the climate during the Late Holocene occurred worldwide (Bond et al., 2001; Rasmussen et al., 2007; Zhu et al., 2009; Marcott et al., 2013). For example, lake shrinkage and salinization has also been observed in Nam Co during 1.4–0.8 kyr BP, and these climate variations have been identified in cores from other glacier-fed lakes, such as Lingge Co on the northern part of the TP based on the paleoshorelines (Pan et al., 2012), Taro Co based on the $\delta^{18}O$ values of ostracod shells (Guo et al., 2016), Buruo Co based on the

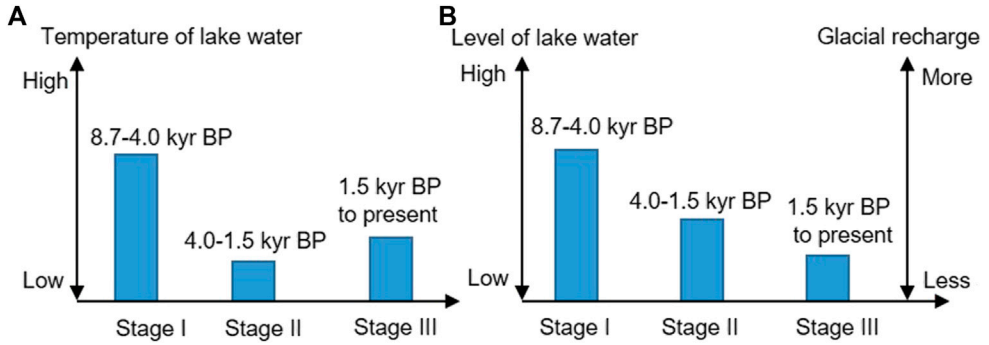

FIGURE 10 | Comparison of **(A)** the temperature changes of the lake water and **(B)** the lake water level changes (Left axis) and the glacial recharge changes (Right axis) during the three stages.

grain size and elements (Xu et al., 2019), and Selin Co based on the shorelines (Shi et al., 2017). The climatic fluctuations in the Late Holocene have also been observed in the western Bay of Bengal (dominated by ISM) based on the reconstructed sea surface temperature (Govil and Naidu, 2011) and in western Australia based on the $\delta^{18}O$ values of stalagmites (Denniston et al., 2013; **Figure 11**).

Based on the presence of aragonite, Guozha Co became a brackish lake at least by 1.5 kyr BP. This is consistent with the adjacent Bangong Co, in which aragonite was found at 1.3 kyr BP (**Figure 11**). Therefore, the recharge from glacial meltwater was low, and the glacier may not have retreated. In this stage, multiple glacier advances occurred in most regions during the Late Holocene (Owen, 2009), including the glaciers in the West Kunlun Mountains (Li, 1996; Thompson et al., 2018).

During the past century, the global temperature began to increase dramatically (**Figure 11**; Marcott et al., 2013). The glaciers in the West Kunlun Mountains retreated from 1976 to 2010 based on remote sensing and the expansion of the glacial lakes on the northern slope of the West Kunlun Mountains (Li et al., 2015). Corresponding to the glaciers retreating, a river flowing from Guozha Co was identified by Li et al. (2021), although the modern lake water in Guozha Co is still brackish (**Table 1**). Therefore, both of the glaciers and lakes in the West Kunlun Mountains are controlled by climatic change, but they exhibit opposite changes.

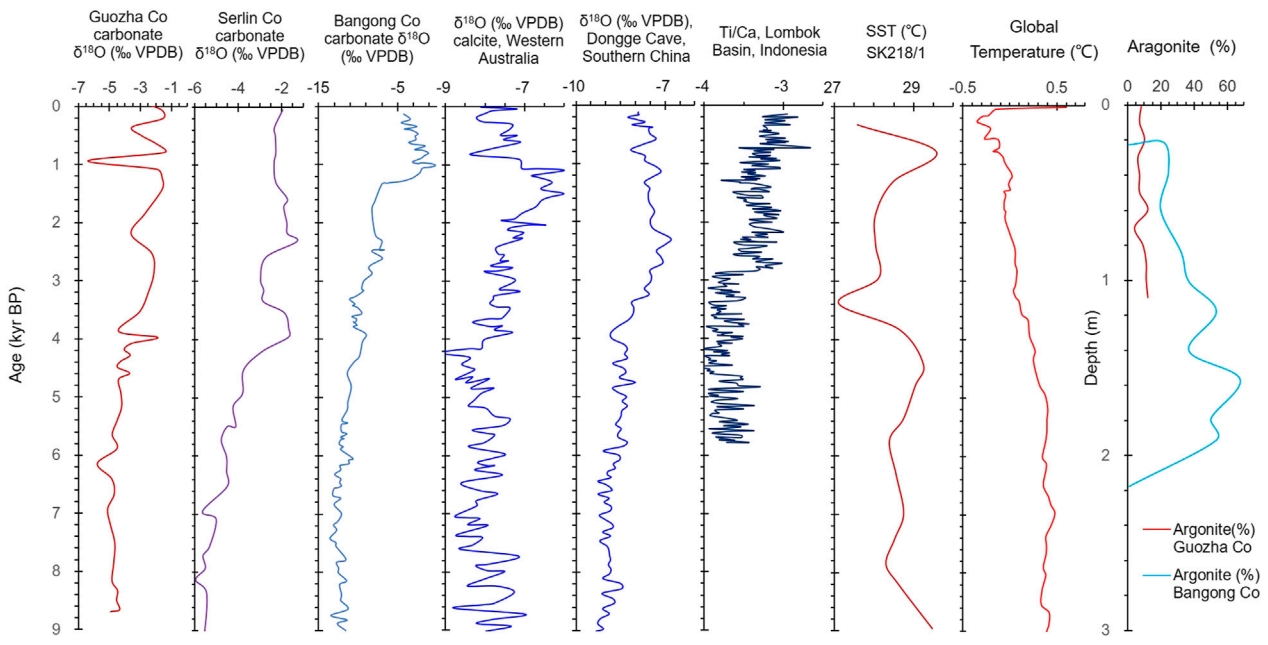

FIGURE 11 | Comparison of data from this study and other records. The $\delta^{18}O$ of sediments carbonate for Bangong Co and Selin Co are from Gasse et al. (1996) and Gu et al. (1993), respectively. The $\delta^{18}O$ of cave carbonate for Western Australia and southern China are from Denniston et al. (2013) and Yuan et al. (2004), respectively. Ti/Ca for Indonesia are from Steinke et al. (2014), the reconstructed SST of marine core SK218/1 from the western Bay of Bengal are from Govil and Naidu (2011), and the aragonite data for Bangong Co are from Fontes et al. (1996). The global temperature data are from Marcott et al. (2013).

CONCLUSION

The carbonates in the Guozha Co sediments are mainly authigenic/endogenic calcite and aragonite. The $\delta^{18}O$-$_{VPDB}$-$\delta^{13}C$-$_{VPDB}$ values of the fine-grained carbonates are slightly more positive than those of the bulk carbonate, and both are controlled by the isotopic composition of the lake water.

Proxies for calcite content, the $\delta^{18}O$-$_{VPDB}$ and $\delta^{13}C$-$_{VPDB}$ values, and their correlation coefficients suggest that three stages occurred at 8.7–4.0, 4.0–1.5, and from 1.5 kyr BP to present, during which the recharge from glacial meltwater decreased.

Guozha Co has been a closed basin since at least 8.7 kyr BP, and it changed from a fresh lake during 8.7–1.5 kyr BP to a brackish lake from 1.5 kyr BP to present, coincident with several climate events, despite the fact that the glacial meltwater diluted the ion concentrations in the lake water. The glacier and the lakes in the West Kunlun Mountains exhibit opposite changes, but both are controlled by climatic changes.

DATA AVAILABILITY STATEMENT

The original contributions presented in the study are included in the article/Supplementary Material. Further inquiries can be directed to the corresponding author.

AUTHOR CONTRIBUTIONS

LZ designs the research, constructs the dating, and writes the text. ML makes the minerals and isotope analyses and writes text. JW, JJ, CL, QM, TX, and BQ carried out field investigation and coring. XW participates in laboratory analyses.

FUNDING

This study was supported by the China Ministry of Science and Technology, the Second Tibetan Plateau Scientific Expedition and Research (grant no. 2019QZKK0202), the Key Project of the National Natural Science Foundation of China (grant no. 41831177), and the Strategic Priority Research Program of the Chinese Academy of Sciences (grant nos. XDA20020100 and XDA20070101).

ACKNOWLEDGMENTS

The authors thank LetPub (www.letpub.com) for its linguistic assistance during the preparation of this article.

REFERENCES

Abell, P. I., and Williams, M. A. J. (1989). Oxygen and Carbon Isotope Ratios in Gastropod Shells as Indicators of Paleoenvironments in the Afar Region of ethiopia. *Palaeogeogr. Palaeoclimatol. Palaeoecol.* 74, 265–278. doi:10.1016/0031-0182(89)90065-5

Bernasconi, S. M., and McKenzie, J. A. (2013). "Carbonate Stable Isotopes Lake Sediments", in *Encyclopedia of Quaternary Science*. Editors Elias, S. A., and Mock, C. J. 2nd Edn, (Elsevier), 333–340.

Bolch, T., Kulkarni, A., Kääb, A., Huggel, C., Paul, F., Cogley, J. G., et al. (2012). The State and Fate of Himalayan Glaciers. *Science* 336, 310–314. doi:10.1126/science.1215828

Bond, G., Kromer, B., Beer, J., Muscheler, R., Evans, M. N., Showers, W., et al. (2001). Persistent Solar Influence on north Atlantic Climate Change during Holocene. *Science* 294 (13), 2130–2135. doi:10.1126/science.1065680

Bond, G., Showers, W., Cheseby, M., Lotti, R., Almasi, P., deMenocal, P., et al. (1997). A Pervasive Millennial-Scale Cycle in North Atlantic Holocene and Glacial Climates. *Science* 278, 1257–1266. doi:10.1126/science.278.5341.1257

Börner, N., De Baere, B., Akita, L. G., Francois, R., Jochum, K. P., Frenzel, P., et al. (2017). Stable Isotopes and Trace Elements in Modern Ostracod Shells: Implications for Reconstructing Past Environments on the Tibetan Plateau, China. *J. Paleolimnol* 58, 191–211. doi:10.1007/s10933-017-9971-1

Bureau of Geology and Mineral resources of Xizang Autonomous Regions (1993). *Regional Geology of Xingzang(Tibet) Autonomous Region*. Beijing: Geological Publishing House.(in Chinese).

Chen, D. L., Xu, B. Q., Yao, T. D., Guo, Z. T., Cui, P., Chen, F. H., et al. (2015). Assessment of Past, Present and Future Environmental Changes on the Tibetan Plateau. *Chin. Sci. Bull.* 60, 3025–3035. doi:10.1360/n972015-00849

Chen, F., Zhang, J., Liu, J., Cao, X., Hou, J., Zhu, L., et al. (2020). Climate Change, Vegetation History, and Landscape Responses on the Tibetan Plateau during the Holocene: a Comprehensive Review. *Quat. Sci. Rev.* 243, 106444. doi:10.1016/j.quascirev.2020.106444

Denniston, R. F., Wyrwoll, K. H., Polyak, V. J., Brown, J. R., Asmerom, Y., Wanamaker, A. D., Jr., et al. (2013). A Stalagmite Record of Holocene Indonesiane Australian Summer Monsoon Variability from the Australian Tropics. *Quat. Sci. Rev.* 78, 155–168. doi:10.1016/j.quascirev.2013.08.004

Deocampo, D. M., and Tactikos, J. C. (2010). Geochemical gradients and artifact mass densities on the lowermost Bed II eastern lake margin (~1.8Ma), Olduvai Gorge, Tanzania. *Quat. Research* 74 (3), 411–423. doi:10.1016/j.yqres.2010.09.004

Digerfeldt, G., Olsson, S., and Sandgren, P. (2000). Reconstruction of lake-level Changes in lake Xinias, central Greece, during the Last 40 000 Years. *Palaeogeogr. Palaeoclimatol. Palaeoecol.* 158 (1), 65–82. doi:10.1016/s0031-0182(00)00029-8

Fontes, J.-C., Gasse, F., and Gibert, E. (1996). Holocene Environmental Changes in Lake Bangong Basin (Western Tibet). Part 1: Chronology and Stable Isotopes of Carbonates of a Holocene Lacustrine Core. *Palaeogeogr. Palaeoclimatol. Palaeoecol.* 120, 25–47. doi:10.1016/0031-0182(95)00032-1

Gasse, F., Fontes, J. C., Van Campo, E., and Wei, K. (1996). Holocene Environmental Changes in Bangong Co Basin (Western Tibet). Part 4: Discussion and Conclusions. *Palaeogeogr. Palaeoclimatol. Palaeoecol.* 120, 79–92. doi:10.1016/0031-0182(95)00035-6

Giosan, L., Clift, P. D., Macklin, M. G., Fuller, D. Q., Constantinescu, S., Durcan, J. A., et al. (2012). Fluvial Landscapes of the Harappan Civilization. *Proc. Natl. Acad. Sci.* 109 (26), E1688–E1694. doi:10.1073/pnas.1112743109

Govil, P., and Divakar Naidu, P. (2011). Variations of Indian Monsoon Precipitation during the Last 32kyr Reflected in the Surface Hydrography of the Western Bay of Bengal. *Quat. Sci. Rev.* 30, 3871–3879. doi:10.1016/j.quascirev.2011.10.004

Grossman, E. L., and Ku, T.-L. (1986). Oxygen and Carbon Isotope Fractionation in Biogenic Aragonite: Temperature Effects. *Chem. Geology. Isotope Geosci. section* 59, 59–74. doi:10.1016/0168-9622(86)90057-6

Gu, Z. Y., Liu, J, Q., Yuan, B. Y., Liu, T. S., Liu, R. M., Liu, Y., et al. (1993). Monsoon Variations of the Qinghai-Xizang Plateau during the Last 12 000 Years: Geochemical Evidences from the Sediments in the Siling Co (lake). *Chinense Sci. Bull.* 07.

Guo, Y., Zhu, L., Frenzel, P., Ma, Q., Ju, J., Peng, P., et al. (2016). Holocene lake Level Fluctuations and Environmental Changes at Taro Co, Southwestern Tibet, Based on Ostracod-Inferred Water Depth Reconstruction. *The Holocene* 26, 29–43. doi:10.1177/0959683615596829

Hardie, L. A., Lowenstein, T. K., and Spencer, R. J. (1985). The Problem of Distinguishing between Primary and Secondary Features in Evaporites. in *Sixth International Symposium on Salt*, 1. Alexandria: Salt Institute, 11–39.

He, Y., Zhao, C., Liu, Z., Wang, H., Liu, W., Yu, Z., et al. (2016). Holocene Climate Controls on Water Isotopic Variations on the Northeastern Tibetan Plateau. *Chem. Geology.* 440, 239–247. doi:10.1016/j.chemgeo.2016.07.024

Henderson, A. C. G., Holmes, J. A., and Leng, M. J. (2010). Late Holocene Isotope Hydrology of Lake Qinghai, NE Tibetan Plateau: Effective Moisture Variability and Atmospheric Circulation Changes. *Quat. Sci. Rev.* 29, 2215–2223. doi:10.1016/j.quascirev.2010.05.019

Horton, T. W., Defliese, W. F., Tripati, A. K., and Oze, C. (2016). Evaporation Induced 18O and 13C Enrichment in lake Systems: A Global Perspective on Hydrologic Balance Effects. *Quat. Sci. Rev.* 131, 365–379. doi:10.1016/j.quascirev.2015.06.030

Hren, M. T., and Sheldon, N. D. (2012). Temporal Variations in lake Water Temperature: Paleoenvironmental Implications of lake Carbonate δ18O and Temperature Records. *Earth Planet. Sci. Lett.* 337-338, 77–84. doi:10.1016/j.epsl.2012.05.019

Kääb, A., Berthier, E., Nuth, C., Gardelle, J., and Arnaud, Y. (2012). Contrasting Patterns of Early Twenty-First-Century Glacier Mass Change in the Himalayas. *Nature* 488, 495–498. doi:10.1038/nature11324

Keatings, K. W., Heaton, T. H. E., and Holmes, J. A. (2002). Carbon and Oxygen Isotope Fractionation in Non-marine Ostracods: Results from a 'natural Culture' Environment. *Geochimica et Cosmochimica Acta* 66, 1701–1711. doi:10.1016/s0016-7037(01)00894-8

Kelts, K. (1988). Environments of Deposition of Lacustrine Petroleum Source Rocks: an Introduction, in *Geological Society*, London, Special Publications 40. 3–26. doi:10.1144/gsl.sp.1988.040.01.02

Kim, S.-T., and O'Neil, J. R. (1997). Equilibrium and Nonequilibrium Oxygen Isotope Effects in Synthetic Carbonates. *Geochimica et Cosmochimica Acta* 61, 3461–3475. doi:10.1016/s0016-7037(97)00169-5

Land, L. S. (1980). The Isotopic and Trace Element Geochemistry of Dolomite: the State of the Art. In: D. H. Zenger, J. B. Dunham, and R. L. Ethington (Eds.), *Concepts and Models of Dolomitization 28*. Broken Arrow: SEPM Special Publication. *pp*. 87–110. doi:10.2110/pec.80.28.0087

Landmann, G., Abu Qudaira, G. M., Shawabkeh, K., Wrede, V., and Kempe, S. (2002). Geochemistry of the Lisan and Damya Formations in Jordan, and Implications for Palaeoclimate. *Quat. Int.* 89, 45–57. doi:10.1016/s1040-6182(01)00080-5

Leng, M. J., and Marshall, J. D. (2004). Palaeoclimate Interpretation of Stable Isotope Data from lake Sediment Archives. *Quat. Sci. Rev.* 23 (7), 811–831. doi:10.1016/j.quascirev.2003.06.012

Li, B. Y., Zhang, Q. S., and Wang, F. B. (1991). Evolution of the Lakes in the KARAKORUM-West Kunlun Mountains. *Quat. Sci.* (1), 64–71. (in Chinese with English abstract).

Li, C.-G., Wang, M., Liu, W., Lee, S.-Y., Chen, F., and Hou, J. (2021). Quantitative Estimates of Holocene Glacier Meltwater Variations on the Western Tibetan Plateau. *Earth Planet. Sci. Lett.* 559, 116766. doi:10.1016/j.epsl.2021.116766

Li, C. X., Yang, T. B., and Tian, H. Z. (2015). Variation of Western Kunlun Mountain Glaciers Monitored by Remote Sensing during 1976—2010. *Mountain Res.* 33 (2), 157–165. (In Chinese with English Abstract). doi:10.16089/j.cnki.1008-2786.000021

Li, J. J. (1996). Climatic Change in Arid Areas of China and Monsoon Fluctuations during the Past 10 K Years. *J. Arid Environ.* 32, 1–7.

Li, M., Kang, S., Zhu, L., Wang, F., Wang, J., Yi, C., et al. (2009). On the Unusual Holocene Carbonate Sediment in lake Nam Co, central Tibet. *J. Mt. Sci.* 6, 346–353. doi:10.1007/s11629-009-1020-8

Li, M., Kang, S., Zhu, L., You, Q., Zhang, Q., and Wang, J. (2008). Mineralogy and Geochemistry of the Holocene Lacustrine Sediments in Nam Co, Tibet. *Quat. Int.* 187, 105–116. doi:10.1016/j.quaint.2007.12.008

Li, M., Wang, J., Zhu, L., Wang, L., and Yi, C. (2012). Distribution and Formation of Monohydrocalcite from Surface Sediments in Nam Co Lake, Tibet. *Quat. Int.* 263, 85–92. doi:10.1016/j.quaint.2012.01.035

Li, M., Zhu, L., Wang, J., Wang, L., Yi, C., and Galy, A. (2011). Multiple Implications of Rare Earth Elements for Holocene Environmental Changes in Nam Co, Tibet. *Quat. Int.* 236, 96–106. doi:10.1016/j.quaint.2010.12.022

Li, S. J., Zheng, B. X., and Jiao, K. Q. (1993). Lakes in the Western Kunlun Moutain Areas. *Oceannol. Liminol. Sinica.* 24 (1), 37–44. (in Chinese with English abstract).

Li, S. J., Zheng, B. X., and Jiao, K. Q. (1991). Preliminary Research on Lacustrine deposit and lake Evolution on the South Slope of the Western Kunlun Mountains. *Scientia Geograp. Sinica.* 11 (4), 308–314. (in Chinese with English abstract). 10.13249/j.cnki.sgs.1991.04.306.

Liu, C., Zhao, Q., and Wang, P. (2001). Correlation between Carbon and Oxygen Isotopic Ratios of Lacustrine Carbonates and Types of Oil-Producing Paleolake. *Geochimica* 30 (4), 363–367. (In Chinese with English abstract). doi:10.19700/j.0379-1726.2001.04.009

Liu, W., Li, X., Zhang, L., An, Z., and Xu, L. (2009). Evaluation of Oxygen Isotopes in Carbonate as an Indicator of lake Evolution in Arid Areas: The Modern Qinghai Lake, Qinghai-Tibet Plateau. *Chem. Geology.* 268, 126–136. doi:10.1016/j.chemgeo.2009.08.004

Liu, X. Q., Shen, J., Wang, S. M., Zhang, E. L., and Cai, Y. F. (2003). A 16000-Year Paleoclimatic Record Derived from Authigenetic Carbonate of Lacustrine Sediment in Qinghai Lake. *Geolog. China Univer.* 9 (1), 38–46. (In Chinese with English abstract). doi:10.16108/j.issn1006-7493.2003.01.005

MacDonald, G. (2011). Potential Influence of the Pacific Ocean on the Indian Summer Monsoon and Harappan Decline. *Quat. Int.* 229 (1–2), 140–148. doi:10.1016/j.quaint.2009.11.012

Marcott, S. A., Shakun, J. D., Clark, P. U., and Mix, A. C. (2013). A Reconstruction of Regional and Global Temperature for the Past 11,300 Years. *Science* 339, 1198–1201. doi:10.1126/science.1228026

McCormack, J., Nehrke, G., Jöns, N., Immenhauser, A., and Kwiecien, O. (2019). Refining the Interpretation of Lacustrine Carbonate Isotope Records: Implications of a Mineralogy-specific Lake Van Case Study. *Chem. Geology.* 513, 167–183. doi:10.1016/j.chemgeo.2019.03.014

Mehrotra, N., Shah, S. K., Basavaiah, N., Laskar, A. H., and Yadava, M. G. (2019). Resonance of the '4.2ka Event' and Terminations of Global Civilizations during the Holocene, in the Palaeoclimate Records Around PT Tso Lake, Eastern Himalaya. *Quat. Int.* 507, 206–216. doi:10.1016/j.quaint.2018.09.027

Morrill, C., Overpeck, J. T., Cole, J. E., Liu, K.-b., Shen, C., and Tang, L. (2006). Holocene Variations in the Asian Monsoon Inferred from the Geochemistry of lake Sediments in central Tibet. *Quat. Res.* 65, 232–243. doi:10.1016/j.yqres.2005.02.014

Mügler, I., Gleixner, G., Günther, F., Mäusbacher, R., Daut, G., Schütt, B., et al. (2010). A Multi-Proxy Approach to Reconstruct Hydrological Changes and Holocene Climate Development of Nam Co, Central Tibet. *J. Paleolimnol* 43, 625–648. doi:10.1007/s10933-009-9357-0

Murphy, J. T., Lowenstein, T. K., and Pietras, J. T. (2014). Preservation of Primary lake Signatures in Alkaline Earth Carbonates of the Eocene Green River Wilkins Peak-Laney Member Transition Zone. *Sediment. Geology.* 314, 75–91. doi:10.1016/j.sedgeo.2014.09.005

Owen, L. A., and Dortch, J. M. (2014). Nature and Timing of Quaternary Glaciation in the Himalayan-Tibetan Orogen. *Quat. Sci. Rev.* 88, 14–54. doi:10.1016/j.quascirev.2013.11.016

Owen, L. A. (2009). Latest Pleistocene and Holocene Glacier Fluctuations in the Himalaya and Tibet. *Quatern. Sci. Rev.* 28 (21-22), 2150–2164. doi:10.1016/j.quascirev.2008.10.020

Pan, B., Yi, C., Jiang, T., Dong, G., Hu, G., and Jin, Y. (2012). Holocene lake-level Changes of Linggo Co in central Tibet. *Quat. Geochronol.* 10, 117–122. doi:10.1016/j.quageo.2012.03.009

Pang, H., Hou, S., Zhang, W., Wu, S., Jenk, T. M., Schwikowski, M., et al. (2020). Temperature Trends in the Northwestern Tibetan Plateau Constrained by Ice Core Water Isotopes over the Past 7,000 Years. *J. Geophys. Res. Atmos.* 125, e2020JD032560. doi:10.1029/2020jd032560

Qiao, B., and Zhu, L. (2019). Difference and Cause Analysis of Water Storage Changes for Glacier-Fed and Non-glacier-fed Lakes on the Tibetan Plateau. *Sci. Total Environ.* 693, 133399. doi:10.1016/j.scitotenv.2019.07.205

Qiao, B., Zhu, L., Wang, J., Ju, J., Ma, Q., and Liu, C. (2017). Estimation of Lakes Water Storage and Their Changes on the Northwestern Tibetan Plateau Based on Bathymetric and Landsat Data and Driving Force Analyses. *Quat. Int.* 454, 56–67. doi:10.1016/j.quaint.2017.08.005

Rao, W., Chen, J., Yang, J., Ji, J., and Zhang, G. (2009). Sr Isotopic and Elemental Characteristics of Calcites in the Chinese Deserts: Implications for Eolian Sr

Transport and Seawater Sr Evolution. *Geochimica et Cosmochimica Acta* 73, 5600–5618. doi:10.1016/j.gca.2009.06.028

Rasmussen, S. O., Vinther, B. M., Clausen, H. B., and Anderson, K. K. (2007). Early Holocene Climate Oscillations Recorded in Three Greenland Ice Cores. *Quat. Sci. Rev.* 26 (3), 1907–1914. doi:10.1016/j.quascirev.2007.06.015

Reimer, P. J., Bard, E., Bayliss, A., Beck, J. W., Blackwell, P. G., Ramsey, C. B., et al. (2013). IntCal13 and Marine13 Radiocarbon Age Calibration Curves 0-50,000 Years Cal BP. *Radiocarbon* 55 (4), 1869–1887. doi:10.2458/azu_js_rc.55.16947

Rivadeneyra, M. A., Martín-Algarra, A., Sánchez-Navas, A., and Martín-Ramos, D. (2006). Carbonate and Phosphate Precipitation byChromohalobacter Marismortui. *Geomicrobiology J.* 23 (1), 1–13. doi:10.1080/01490450500398245

Shapley, M. D., Ito, E., and Donovan, J. J. (2005). Authigenic Calcium Carbonate Flux in Groundwater-Controlled Lakes: Implications for Lacustrine Paleoclimate Records. *Geochimica et Cosmochimica Acta* 69 (10), 2517–2533. doi:10.1016/j.gca.2004.12.001

Shen, J., Liu, X. Q., aWang, S. M., and Matsumoto, R. (2005). Palaeoclimatic Changes in the Qinghai Lake Area during the Last 18,000 Years. *Quatern. Internat.* 136 (1), 131–140. doi:10.1016/j.quaint.2004.11.014

Shi, X., Kirby, E., Furlong, K. P., Meng, K., Robinson, R., Lu, H., et al. (2017). Rapid and Punctuated Late Holocene Recession of Siling Co, central Tibet. *Quat. Sci. Rev.* 172, 15–31. doi:10.1016/j.quascirev.2017.07.017

Solomina, O. N., Bradley, R. S., Hodgson, D. A., Ivy-Ochs, S., Jomelli, V., Mackintosh, A. N., et al. (2015). Holocene Glacier Fluctuations. *Quat. Sci. Rev.* 111, 9–34. doi:10.1016/j.quascirev.2014.11.018

Steinke, S., Mohtadi, M., Prange, M., Varma, V., Pittauerova, D., and Fischer, H. W. (2014). Mid- to Late-Holocene Australian-Indonesian Summer Monsoon Variability. *Quat. Sci. Rev.* 93, 142–154. doi:10.1016/j.quascirev.2014.04.006

Talbot, M. R. (1990). A Review of the Palaeohydrological Interpretation of Carbon and Oxygen Isotopic Ratios in Primary Lacustrine Carbonates. *Chem. Geology. Isotope Geosci. section* 80 (4), 261–279. doi:10.1016/0168-9622(90)90009-2

Thompson, L. G. (2000). Ice Core Evidence for Climate Change in the Tropics: Implications for Our Future. *Quat. Sci. Rev.* 19 (1–5), 19–35. doi:10.1016/s0277-3791(99)00052-9

Thompson, L. G., Yao, T., Davis, M. E., Henderson, K. A., Mosley-Thompson, E., Lin, P.-N., et al. (1997). Tropical Climate Instability: the Last Glacial Cycle from a Qinghai-Tibetan Ice Core. *Science* 276, 1821–1825. doi:10.1126/science.276.5320.1821

Thompson, L. G., Yao, T., Davis, M. E., Mosley-Thompson, E., Wu, G., Porter, S. E., et al. (2018). Ice Core Records of Climate Variability on the Third Pole with Emphasis on the Guliya Ice Cap, Western Kunlun Mountains. *Quat. Sci. Rev.* 188, 1–14. doi:10.1016/j.quascirev.2018.03.003

Wang, N., Liu, W. G., Xu, L. M., and An, Z. S. (2008). Oxygen Isotopic Compositions of Carbonates of Modern Surface Lacustrine Sediments and Their Affecting Factors in Tibet Plateau. *Quatern. Sci.* 28, 591–600.

Wang, Z., Gaetani, G., Liu, C., and Cohen, A. (2013). Oxygen Isotope Fractionation between Aragonite and Seawater: Developing a Novel Kinetic Oxygen Isotope Fractionation Model. *Geochimica et Cosmochimica Acta* 117, 232–251. doi:10.1016/j.gca.2013.04.025

Warren, J. (2000). Dolomite: Occurrence, Evolution and Economically Important Associations. *Earth Sci. Rev.* 52, 1–81. doi:10.1016/s0012-8252(00)00022-2

Warren, J. K. (1989). *Evaporite Sedimentology: Importance in Hydrocarbon Accumulation*. Englewood Cliffs, NJ: Prentice-Hall, 1–37.

Wei, K., and Gasse, F. (1999). Oxygen Isotopes in Lacustrine Carbonates of West China Revisited: Implications for post Glacial Changes in Summer Monsoon Circulation. *Quat. Sci. Rev.* 18, 1315–1334. doi:10.1016/s0277-3791(98)00115-2

Wünnemann, B., Yan, D., Andersen, N., Riedel, F., Zhang, Y., Sun, Q., et al. (2018). A 14 Ka High-Resolution δ18O lake Record Reveals a Paradigm Shift for the Process-Based Reconstruction of Hydroclimate on the Northern Tibetan Plateau. *Quat. Sci. Rev.* 200, 65–84. doi:10.1016/j.quascirev.2018.09.040

Xiao, J., Zhang, S., Fan, J., Wen, R., Xu, Q., Inouchi, Y., et al. (2019). The 4.2 Ka Event and its Resulting Cultural Interruption in the Daihai Lake basin at the East Asian Summer Monsoon Margin. *Quat. Int.* 527, 87–93. doi:10.1016/j.quaint.2018.06.025

Xu, T., Zhu, L., Lü, X., Ma, Q., Wang, J., Ju, J., et al. (2019). Mid- to Late-Holocene Paleoenvironmental Changes and Glacier Fluctuations Reconstructed from the Sediments of Proglacial lake Buruo Co, Northern Tibetan Plateau. *Palaeogeogr. Palaeoclimatol. Palaeoecol.* 517, 74–85. doi:10.1016/j.palaeo.2018.12.023

Xu, X., and Yi, C. (2017). Timing and Configuration of the Gongga II Glaciation in the Hailuogou valley, Eastern Tibetan Plateau: A Glacier-Climate Modeling Method. *Quat. Int.* 444, 151–156. doi:10.1016/j.quaint.2017.01.011

Yang, M., Yao, T., Wang, H., and Gou, X. (2006). Climatic Oscillations over the Past 120kyr Recorded in the Guliya Ice Core, China. *Quat. Int.* 154-155, 11–18. doi:10.1016/j.quaint.2006.02.015

Yang, R. M., Zhu, L. P., Wang, J. B., Ju, J. T., Ma, Q. F., Turner, F., et al. (2017). Spatiotemporal Variations in Volume of Closed Lakes on the Tibetan Plateau and Their Climatic Responses from 1976 to 2013. *Climatic Change* 140 (3-4), 621–633. doi:10.1007/s10584-016-1877-9

Yao, T., Masson-Delmotte, V., Gao, J., Yu, W., Yang, X., Risi, C., et al. (2013). A Review of Climatic Controls on δ18O in Precipitation over the Tibetan Plateau: Observations and Simulations. *Rev. Geophys.* 51, 525–548. doi:10.1002/rog.20023

Yao, T., Thompson, L., Yang, W., Yu, W., Gao, Y., Guo, X., et al. (2012). Different Glacier Status with Atmospheric Circulations in Tibetan Plateau and Surroundings. *Nat. Clim Change* 2 (9), 663–667. doi:10.1038/nclimate1580

Yao, T., Xue, Y., Chen, D., Chen, F., Thompson, L., Cui, P., et al. (2019). Recent Third Pole's Rapid Warming Accompanies Cryospheric Melt and Water Cycle Intensification and Interactions between Monsoon and Environment: Multidisciplinary Approach with Observations, Modeling, and Analysis. *Bull. Am. Meteorolog. Soc.* 100 (3), 423–444. doi:10.1175/bams-d-17-0057.1

Yu, W. S., Tian, L. D., Risi, C., Yao, T. D., Ma, Y. M., Zhao, H. B., et al. (2016). $\delta^{18}O$ Records in Water Vapor and an Ice Core from the Eastern Pamir Plateau: Implications for Paleoclimate Reconstructions. *Earth Planetary Sci. Lett.* 456, 146–156. doi:10.1016/j.epsl.2016.10.001

Yuan, D., Cheng, H., Edwards, R. L., Dykoski, C. A., Kelly, M. J., Zhang, M. L., et al. (2004). Timing, Duration, and Transitions of the Last Interglacial Asian Monsoon. *Science* 304, 575–578. doi:10.1126/science.1091220

Zheng, D. (1996). The System of Physico-Geographical Regions of the Qinghai-Xizang (Tibet) Plateau. *Sci. China Ser. D-Earth Sci.* 39 (4), 410–417.

Zheng, X. Y., Zhang, M. G., Xu, C., and Li, B. X. (2002). *Salt Lake of China*. Beijing: China Science Press.

Zhu, L., Wang, J., Lin, X., Ju, J. T., Xie, M. P., Li, M. H., et al. (2008). Environmental Changes Reflected by Core Sediments since 8.4 Ka in Nam Co, Central Tibet of China. *Holocene* 185, 831–839. doi:10.1177/0959683608091801

Zhu, L., Zhen, X., Wang, J., Lü, H., Xie, M., Kitagawa, H., et al. (2009). A ~30,000-year Record of Environmental Changes Inferred from Lake Chen Co, Southern Tibet. *J. Paleolimnol.* 42, 343–358. doi:10.1007/s10933-008-9280-9

Conflict of Interest: The authors declare that the research was conducted in the absence of any commercial or financial relationships that could be construed as a potential conflict of interest.